5456 *Chem. Mater.* **2009,** *21,* 5456–5465
DOI:10.1021/cm902229x

CHEMISTRY OF MATERIALS
Article

Synthesis of Bi_2S_3 Nanostructures from Bismuth(III) Thiourea and Thiosemicarbazide Complexes

Vitalie Stavila,[†] Kenton H. Whitmire,*[,†] and Irene Rusakova[‡]

[†]*Department of Chemistry, MS 60, Rice University, 6100, Main Street, Houston, Texas 77005-1892, and* [‡]*Texas Center for Superconductivity, University of Houston, Houston, Texas 77204-5931*

Received July 21, 2009. Revised Manuscript Received September 14, 2009

Rod-shaped nanostructures of Bi_2S_3 were synthesized by the solution decomposition of the two new bismuth(III) complexes $[Bi_6(pydc)_8(Hpydc)_2(tu)_8]$ (**1**) and $\{[Bi_2(pydc)_3(tsc)(H_2O)_2]\cdot H_2O\}_\infty$ (**2**) (H_2pydc = 2,6-pyridinedicarboxylic acid also known as dipicolinic acid; tu = thiourea, tsc = thiosemicarbazide). They were obtained by treatment of Bi_2O_3 with dipicolinic acid in the presence of the sulfur-containing ligands. The complexes were characterized with the aid of elemental analysis, IR spectroscopy, and single-crystal X-ray diffraction. The dipicolinate anions behave as tridentate ligands toward Bi(III), but two modes of coordination are found. In both cases the ligand serves as a pincer ligand O,N,O-bonded to one bismuth(III) center, but it can also function as a bridging ligand through one carboxylate group that assembles into hexanuclear molecules (**1**) or a polymeric chain (**2**). The air-stable complexes **1** and **2** have been used as starting materials in the preparation of bismuth sulfide nanoparticles (NPs) in the presence of different surfactants. Decomposition of **1** and **2** gave Bi_2S_3 in all cases, but addition of a small amount of 1-dodecanethiol (DT) or 1-octadecanethiol (OT) at 120 °C resulted in better crystallite growth with the observation of nanorods up to several hundreds of nanometers in length. These were examined by scanning electron microscopy (SEM) and transmission electron microscopy (TEM). The influence of various reaction conditions on the shape and size of the nanocrystals is discussed. The high resolution (HR) TEM images reveal a number of linear and planar crystal defects and atomic distortions that account for the splitting of bismuth sulfide nanocrystals as observed previously. The growth mechanism is believed to involve decomposition of the precursors and formation of Bi_2S_3 seeds, followed by the preferential [001] growth of larger particles. Crystal splitting caused by defects and atomic distortions as well as Ostwald ripening processes play important roles in shaping the morphologies of the final Bi_2S_3 nanostructures.

Introduction

Over the past decade semiconductor nanoparticles (NPs) have attracted increasing interest in virtually all areas of nanoscience and nanotechnology. Their tunable optical and electronic properties make them suitable in many applications, including photonic, photovoltaic, light-emitting, and photoluminescence devices. Orthorhombic bismuth sulfide[1] is an important semiconductor with the direct gap band energy of 1.3 to 1.7 eV and finds application in thermoelectric, electronic, and optoelectronic devices. Thin-films of Bi_2S_3 are good light-harvesting substrates with absorption in the visible and near-IR part of the solar spectrum, which allows their applications in photodiode arrays and photovoltaic converters.[2−4] Recently Rabin et al. proposed the use of polymer-coated Bi_2S_3 nanoparticles as an injectable X-ray computed tomography imaging agent, which could open new directions for applications of bismuth-containing nanomaterials.[5] Cademartiri et al. have recently demonstrated that long Bi_2S_3 nanowires with a necklace architecture show quantum confinement effects.[6]

One of the keys to the successful use of such nanomaterials is the ability to tailor their morphology, composition, and structure, as well as to control size-dispersion and surface functionality. Nanorods, nanowires, and nanotubes have been shown to exhibit superior electrical, optical, mechanical, and thermal properties and provide fundamental building blocks for nanoscale science and technology.[7] A number of strategies have been described in the literature to produce anisotropic nanostructured materials through chemical routes by rational design and

*To whom correspondence should be addressed. E-mail: whitmir@rice.edu. Phone: 713-348-5650. Fax: 713-348-5155.

(1) Black, J.; Conwell, E. M.; Seigle, L.; Spencer, C. W. *J. Phys. Chem. Solids* **1957**, *2*, 240–251.
(2) Mane, R. S.; Sankapal, B. R.; Lokhande, C. D. *Mater. Chem. Phys.* **1999**, *60*, 158–162.
(3) Suarez, R.; Nair, P. K.; Kamat, P. V. *Langmuir* **1998**, *14*, 3236–3241.
(4) Nair, P. K.; Nair, M. T. S.; García, V. M.; Arenas, O. L.; Peña, A. C. Y.; Ayala, I. T.; Gomezdaza, O.; Sánchez, A.; Campos, J.; Hu, H.; Suárez, R.; Rincón, M. E. *Sol. Energy Mater. Sol. Cells* **1998**, *52*, 313–344.
(5) Rabin, O.; Manuel Perez, J.; Grimm, J.; Wojtkiewicz, G.; Weissleder, R. *Nat. Mater.* **2006**, *5*, 118–122.
(6) Cademartiri, L.; Malakooti, R.; O'Brien, P. G.; Migliori, A.; Petrov, S.; Kherani, N. P.; Ozin, G. A. *Angew. Chem., Int. Ed.* **2008**, *47*, 3814–3817.
(7) Xia, Y.; Yang, P.; Sun, Y.; Wu, Y.; Mayers, B.; Gates, B.; Yin, Y.; Kim, F.; Yan, H. *Adv. Mater.* **2003**, *15*, 353–389.

 Published on Web 10/28/2009

tuning the process parameters.[7−10] These soft approaches allow a more homogeneous distribution of elements at the atomic level and a better control over the reaction product during the synthesis.

In situ reaction of inorganic bismuth complexes with sulfur-containing species readily yields bismuth sulfide nanoparticles. Zhou et al. described a polyethylene glycol (PEG)-assisted approach to the large-scale hollow organization of bismuth sulfide nanorods, formed by a hydrothermal reaction between Bi−PEG complexes and thiourea.[11] Christian and O'Brien prepared rod-like particles of Bi_2S_3 by treating bismuth(III) acetate with elemental sulfur under reflux conditions in octylamine.[12] Flowerlike patterns of Bi_2S_3 were synthesized by using L-cysteine, which serves as both the S source and the directing molecule in the formation of Bi_2S_3 nanostructures.[13] Uniform Bi_2S_3 flowers with a size of 3−5 μm composed of nanowires with a diameter of 80 nm can be prepared from $BiCl_3$ and acetothioamide in the presence of the ionic liquid 1-butyl-3-methylimidazolium tetrafluoroborate.[14] Other strategies to produce Bi_2S_3 nanostructures have been described.[6,15−28]

It is almost certain that the conversion to nanoparticles in these systems involves prior coordination of the S-based ligand, and decomposition of preassembled sulfur-containing bismuth(III) complexes may afford some advantages in control over the shape and size of the particles formed.[15−21] Bismuth(III) routinely adopts coordination numbers higher than six and stable aminopolycarboxylate (APC) and polyaminopolycarboxylate (PAPC) complexes that also contain sulfur-based ligands have been reported.[29] Tian et al.[15] have recently reported a colloidal solution method to prepare Bi_2S_3 nanorods and dandelion-like nanostructures from $Bi(SCOPh)_3$ in binary surfactant systems at 150 °C. Han et al.[16] synthesized pyridine and 1,10-phenanthroline adducts of $Bi(S_2COCH(CH_3)CH_2CH_3)_3$ and used the hydrothermal method to convert them to Bi_2S_3 nanorods with diameters ranging from 20 to 35 nm and lengths of hundreds of nanometers in the presence of PVP (PVP = poly(vinyl pyrrolidone)). Bismuth sulfide nanorods with diameters of 7−21 nm and lengths of several hundred nanometers were fabricated by the solvothermal treatment of bismuth(III) di-*n*-octyl-dithiophosphate, $Bi[S_2P(OC_8H_{17})_2]_3$.[17] Rodlike bismuthinite submicrometer particles were prepared from $Bi(S_2CNEt_2)_3$ via a hydrothermal treatment,[20] while $[MeBi(S_2CNR_2)_2]$[19] and $Bi(SCH_2C_6H_5)_3$[21] were shown to produce Bi_2S_3 under mild thermal conditions. Bi_2S_3 nanotubes with cross-sectional width of 100−500 nm were successfully synthesized by Shen et al.[18] from $Bi(S_2CNEt_2)_3$ at 530 °C. The mechanism by which the sulfur compounds decompose is not understood either for in situ preparations or with using single-source precursors.

Although a number of single-source precursors for Bi_2S_3 NPs have been reported in the literature to date, the synthesis of the precursors is quite complex, and in many cases expensive reagents are required. In this article, we describe the facile synthesis of the new air-stable complexes $[Bi_6(pydc)_8(Hpydc)_2(tu)_8]$ (**1**) and $\{[Bi_2(pydc)_3(tsc)(H_2O)_2]\cdot H_2O\}_\infty$ (**2**) and their conversion to Bi_2S_3 NPs in both aqueous and nonaqueous media.

Experimental Section

Materials, Equipment, and Characterization Details. All starting materials and solvents were reagent grade and obtained from commercial sources. The infrared data (IR) were recorded on a Nicolet 670 FT-IR spectrometer using attenuated total reflectance (ATR). CH analyses of the complexes were performed at the Galbraith Laboratories. Transmission electron microscope (TEM) study was carried out using JEOL 2000FX and JEOL 2010 TEM microscopes equipped with energy dispersive spectrometers (EDS) and operating at 200 kV. After resuspending the isolated NPs in toluene or hexane, the TEM samples were prepared by dropping the suspension on a carbon coated 200 mesh copper grid. Scanning electron microscopy (SEM) was performed using a FEI XL-30 environmental scanning electron microscope (ESEM). X-ray diffraction (XRD) data were obtained with a powder diffractometer (Rigaku D/Max-2100PC) using unfiltered Cu Kα radiation (λ = 1.5406 Å) at 40 kV and 40 mA. The contribution from Kα_2 radiation was stripped using the Rachinger algorithm. Goniometer alignment was verified by daily analysis of a Rigaku-supplied SiO_2 reference standard. The processing of the powder diffraction results and phase identification was accomplished using the program JADE.

Synthesis of $[Bi_6(pydc)_8(Hpydc)_2(tu)_8]$, 1. Bismuth(III) oxide (466 mg, 1.0 mmol) and 2,6-pyridinedicarboxylic acid (H_2pydc, 668 mg, 4.0 mmol) were stirred at reflux in water until the dissolution of most of the oxide. Thiourea (304 mg, 4.0 mmol) dissolved in 15 mL of hot H_2O was added, and the solution was

(8) Pickett, N. L.; O'Brien, P. *Chem. Rec.* **2001**, *1*, 467–479.
(9) Soler-Illia, G. J. d. A. A.; Sanchez, C.; Lebeau, B.; Patarin, J. *Chem. Rev.* **2002**, *102*, 4093–4138.
(10) Revaprasadu, N.; Mlondo, S. N. *Pure Appl. Chem.* **2006**, *78*, 1691–1702.
(11) Zhou, X.; Zhao, X.; Zhang, D.; Chen, S.; Guo, X.; Ding, W.; Chen, Y. *Nanotechnology* **2006**, *17*, 3806–3811.
(12) Christian, P.; O'Brien, P. *J. Mater. Chem.* **2005**, *15*, 3021–3025.
(13) Zhang, B.; Ye, X. C.; Hou, W. Y.; Zhao, Y.; Xie, Y. *J. Phys. Chem. B* **2006**, *110*, 8978–8985.
(14) Jiang, J.; Yu, S. H.; Yao, W. T.; Ge, H.; Zhang, G. Z. *Chem. Mater.* **2005**, *17*, 6094–6100.
(15) Tian, L.; Yao Tan, H.; Vittal, J. J. *Cryst. Growth Des.* **2008**, *8*, 734–738.
(16) Han, Q. F.; Chen, J.; Yang, X. J.; Lu, L.; Wang, X. *J. Phys. Chem. C* **2007**, *111*, 14072–14077.
(17) Lou, W.; Chen, M.; Wang, X.; Liu, W. *Chem. Mater.* **2007**, *19*, 872–878.
(18) Shen, X.-P.; Yin, G.; Zhang, W.-L.; Xu, Z. *Solid State Commun.* **2006**, *140*, 116–119.
(19) Jain, A. K.; Sharma, V.; Bohra, R.; Sukumar, A. A.; Raju, V. S.; Drake, J. E.; Hursthouse, M. B.; Light, M. E. *J. Organomet. Chem.* **2006**, *691*, 4128–4134.
(20) Xie, G.; Qiao, Z. P.; Zeng, M. H.; Chen, X. M.; Gao, S. L. *Cryst. Growth Des.* **2004**, *4*, 513–516.
(21) Boudjouk, P.; Remington, M. P.; Grier, D. G.; Jarabek, B. R.; McCarthy, G. J. *Inorg. Chem.* **1998**, *37*, 3538–3541.
(22) Li, L. S.; Sun, N. J.; Huang, Y. Y.; Qin, Y.; Zhao, N.; Gao, J. N.; Li, M. X.; Zhou, H. H.; Qi, L. M. *Adv. Funct. Mater.* **2008**, *18*, 1194–1201.
(23) Alemi, A.; Dolatyari, M. *Radiation Effects Defects Sol.* **2008**, *163*, 123–130.
(24) Li, W. H. *Mater. Lett.* **2008**, *62*, 243–245.
(25) Ota, J.; Srivastava, S. K. *J. Phys. Chem. C* **2007**, *111*, 12260–12264.
(26) Xu, J.; Petkov, N.; Wu, X.; Iacopino, D.; Quinn, A. J.; Redmond, G.; Bein, T.; Morris, M. A.; Holmes, J. D. *ChemPhysChem* **2007**, *8*, 235–240.
(27) Jain, A. K.; Bohra, R. *Appl. Organomet. Chem.* **2006**, *20*, 411–415.
(28) Tang, J.; Alivisatos, A. P. *Nano Lett.* **2006**, *6*, 2701–2706.
(29) Stavila, V.; Davidovich, R. L.; Gulea, A.; Whitmire, K. H. *Coord. Chem. Rev.* **2006**, *250*, 2782–2810.

concentrated to ~1/8 of its initial volume and filtered. The resulting clear solution was left for crystallization for 2 weeks during which time light-yellow crystals of **1** deposited. The product was washed with diethyl ether and dried under vacuum. Yield, ~860 mg, 73% based on Bi. Anal. Found % (Calcd %) for $C_{39}H_{34}Bi_3N_{13}O_{21}S_4$: C, 26.53 (26.64); H, 2.01 (1. 83). ATR (selected bands, cm^{-1}): 3427 (m), 3340 (s), 3285 (s. br), 3123 (s) ν(OH) + ν(NH); 1705 (sh), 1653 (vs br), 1619 (vs br), 1596 (sh) ν_{as}(COO) + δ(NH); 1430 (sh), 1418 (vs br), 1392 (m) ν_s(COO) + ν(CS); 1281 (m, br), 1251 (w), 1138 (w), 1091 (vw), 962 (m), 839 (w), 762 (w), 723 (s), 673 (m), 631 (w), 618 (sh), 597 (vw), 562 (w).

Synthesis of $\{[Bi_2(pydc)_3(tsc)(H_2O)_2]\cdot H_2O\}_\infty$, 2. An aqueous solution obtained by dissolution upon heating of Bi_2O_3 (466 mg, 1.0 mmol) and H_2pydc (668 mg, 4.0 mmol) was treated with a hot aqueous solution of thiosemicarbazide (365 mg, 4.0 mmol) and then concentrated to ~1/10 of the original volume. The filtered clear solution was left for crystallization. A slight yellow product was collected after 8 days and washed with diethyl ether, yielding ~720 mg (68%). Anal. Found % (Calcd %) for $C_{22}H_{20}Bi_2N_6O_{15}S$: C, 25.12 (24.96); H, 2.05 (1.90). ATR (selected bands, cm^{-1}): 3458 (m), 3318 (s), 3236 (s. br), 3153 (s) ν(OH) + ν(NH), 1640 (sh), 1626 (vs br), 1602 (sh), ν_{as}(COO) + δ(NH); 1434 (sh), 1415 (vs br), 1383 (s) ν_s(COO) + ν(CS); 1316 (m), 1283 (m, br), 1249 (w), 1146 (w), 1097 (w), 1007 (w), 961 (m), 841 (w), 764 (w), 711 (s), 644 (w), 603 (vw), 581 (w), 558 (w).

Solution Decomposition. In a typical experiment, 250 mg of the complex was suspended in 5 mL of the solvent (anisole or oleylamine) and added to a hot solution containing 15 mL of that solvent and 0.50 mL of 1-dodecanethiol (DT) (or 550 mg 1-octadecanethiol (OT)) heated upon strong stirring to 120 °C. Bi_2S_3 nanomaterial formation can be followed by the color change of reaction contents, from light yellow to black. After the reaction was finished, the solution was washed several times with ethanol. The Bi_2S_3 NPs were suspended in hexane, and TEM grids were prepared from that suspension. The particles can be redispersed in toluene, hexanes, and chlorinated solvents, such as $CHCl_3$ and CH_2Cl_2.

Hydrothermal Decomposition. A typical synthesis method is as follows. A total of 250 mg of the corresponding complex, 0.200 g of cetyl trimethylammonium bromide (CTAB), and 14 mL of water were mixed with stirring for 30 min. The mixture was then sealed in a 20-mL stainless-steel reactor equipped with a Teflon liner and heated at 175 °C for 4 h. After cooling to room temperature, the dark-brown precipitate of Bi_2S_3 was collected and washed several times by centrifugation with water and ethanol.

Solvothermal Decomposition. The appropriate complex (250 mg) was placed in a Teflon reaction vessel fitted in a stainless steel reactor and a mixture containing 10 mL of oleylamine, 2 mL of oleic acid, and 0.50 mL DT was added. The vessel was sealed and placed in the oven at 175 °C for 30 min. The reaction mixture was allowed to cool to room temperature; then the reactor was opened and the resulting black product washed with ethanol. The precipitate can be redispersed in organic solvents with the aid of sonification.

X-ray Structural Determinations. Single-crystals of **1** and **2** suitable for X-ray crystallography were separated as small blocks directly from the aqueous solutions of **1** and **2**. Data were collected at 295(2) K using a Bruker SMART 1000 CCD diffractometer equipped with a Mo-target X-ray tube in a hemisphere with 10 s exposure times. A preliminary search of reciprocal space revealed a triclinic unit cell for both **1** and **2**; the choice of the space group was confirmed by the subsequent solution and refinement of the structures. A full hemisphere of data was collected using the ω-scan method (0.3° frame width). The first 50 frames were remeasured at the end of data collection to monitor instrument and crystal stability. Analysis of the data showed negligible decay during data collection experiments. The frames were integrated with the Bruker SAINT software package and corrected for absorption effects using the empirical method (SADABS). The structures were solved using a combination of direct methods and Fourier techniques and refined by full-matrix least-squares on F^2 using the Bruker SHELXL software package. The coordinates of bismuth and sulfur atoms were found in direct method E maps. The remaining atoms were located after an alternative series of least-squares difference-Fourier cycles. All hydrogen atoms (except for those on the water molecules) were calculated in idealized positions on their respective carbon or nitrogen atoms. The water H atoms were not found in any difference Fourier map. Anisotropic displacement parameters were assigned to all non-H atoms. Table 1 lists the unit cell and structure refinement data for **1** and **2**. Selected bond distances and angles are presented in Table 2.

Table 1. Crystallographic Data for 1 and 2

	1	**2**
formula	$C_{78}H_{64}Bi_6N_{26}O_{40}S_8$	$C_{11}H_{10}BiN_3O_{7.5}S_{0.5}$
Fw	3519.91	529.23
cryst syst	triclinic	triclinic
space group	$P\bar{1}$	$P\bar{1}$
a (Å)	11.377(2)	8.024(2)
b (Å)	15.472(3)	16.952(3)
c (Å)	16.952(3)	18.892(4)
α (deg)	78.328(3)	78.10(3)
β (deg)	75.912(3)	78.59(3)
γ (deg)	72.344(3)	76.55(3)
V (Å^3)	2731.1(9)	1465.0(6)
Z	1	4
D_{calcd} ($g\cdot cm^{-3}$)	2.138	2.399
λ (Mo Kα) (Å)	0.71073	0.71073
T (K)	294(1)	294(1)
$2\theta_{max}$ (deg)	51.762	56.62
abs. coeff, mm^{-1}	9.879	12.151
no. of data collected	32127	8983
unique reflections	12764	3731
no. of params refined	717	433
F(000)	1660	992
R_1 [$I > 2\sigma(I)$]	0.0727	0.0284
crystal size, mm	0.12 × 0.04 × 0.03	0.14 × 0.12 × 0.09
wR_2 [$I > 2\sigma(I)$]	0.1487	0.0741
GOF	0.881	1.026
ρ_{fin}(max/min) ($e^-\cdot$Å^3)	0.45/-0.38	1.06/-0.80

Results and Discussion

Synthesis and Characterization of the Precursor Compounds. Mixed-ligand carboxylate-thiourea (tu) or thiosemicarbazide (tsc) bismuth(III) complexes were prepared in aqueous solutions by the reaction of Bi_2O_3 with 2,6-pyridinedicarboxylic acid (H_2pydc) in the presence of tu or tsc. The compounds were isolated in good yield as air-stable compounds. Even though a 1:2 Bi:S molar ratio was employed for both tu and tsc reactions, the products crystallized with less sulfur-based ligand per bismuth atom than anticipated. Of the two complexes, compound **1** has a closer Bi:S (6:8) ratio to the stoichiometry of Bi_2S_3 (6:9).

The characterization of the complexes was performed using elemental analysis, IR spectroscopy, and single-crystal X-ray diffraction. IR spectra of **1** and **2** show strong bands in the region of 3120−3460 cm^{-1}, which are

Table 2. Selected bond lengths (Å) and angles (deg) for 1 and 2

1				2			
Bi(1)−S(1)	2.743(5)	Bi(2)−O(41)	2.52(1)	Bi(1)−S(1)	2.670(2)	Bi(2)−N(2)	2.412(6)
Bi(1)−N(1)	2.43(1)	Bi(2)−O(43)	2.38(1)	Bi(1)−N(13)	2.619(7)	Bi(2)−O(21)	2.488(5)
Bi(1)−O(11)	2.49(1)	Bi(2)−O(22)	2.50(1)	Bi(1)−N(1)	2.378(7)	Bi(2)−O(23)	2.335(5)
Bi(1)−O(13)	2.34(1)	Bi(2)−O(33A)	2.65(1)	Bi(1)−O(11)	2.278(7)	Bi(2)−N(3)	2.493(7)
Bi(1)−N(2)	2.62(1)	Bi(3)−S(2)	2.809(6)	Bi(1)−O(13)	2.436(6)	Bi(2)−O(31)	2.399(6)
Bi(1)−O(21)	2.58(1)	Bi(3)−S(3)	2.890(7)	Bi(1)−O(21)	2.757(5)	Bi(2)−O(33)	2.591(6)
Bi(1)−O(23)	2.57(1)	Bi(3)−S(4)	2.809(6)	Bi(1)−O(22)	2.653(6)	Bi(2)−O(13B)	2.577(7)
Bi(1)−O(44A)	2.55(1)	Bi(3)−O(42)	2.42(1)	Bi(1)−O(33A)	2.735(6)	Bi(2)−O(1)	2.666(5)
Bi(2)−N(3)	2.45(1)	Bi(3)−O(51)	2.43(1)	N(1)−Bi(1)−S(1)	76.24(15)	Bi(2)−O(2)	2.945(7)
Bi(2)−O(31)	2.29(1)	Bi(3)−O(53)	2.48(1)	O(11)−Bi(1)−S(1)	86.4(2)	N(2)−Bi(2)−O(21)	65.0(2)
Bi(2)−O(33)	2.54(1)	Bi(3)−N(5)	2.51(1)	O(13)−Bi(1)−S(1)	83.1(2)	O(23)−Bi(2)−N(2)	68.6(2)
Bi(2)−N(4)	2.44(1)	N(3)−Bi(2)−N(4)	123.6(5)	N(13)−Bi(1)−S(1)	70.2(1)	O(31)−Bi(2)−N(2)	70.9(2)
N(1)−Bi(1)−S(1)	89.4(4)	O(31)−Bi(2)−N(3)	68.9(5)	O(22)−Bi(1)−S(1)	147.6(2)	N(2)−Bi(2)−N(3)	127.6(2)
O(11)−Bi(1)−S(1)	83.5(3)	N(3)−Bi(2)−O(33)	63.8(5)	S(1)−Bi(1)−O(21)	151.8(1)	N(2)−Bi(2)−O(33)	138.2(2)
O(13)−Bi(1)−S(1)	90.8(3)	N(3)−Bi(2)−O(22)	77.2(5)	S(1)−Bi(1)−O(33A)	81.5(2)	N(2)−Bi(2)−O(13B)	77.8(2)
O(21)−Bi(1)−S(1)	81.9(3)	O(43)−Bi(2)−N(3)	72.4(5)	O(11)−Bi(1)−N(1)	69.9(2)	N(2)−Bi(2)−O(1)	122.4(2)
O(23)−Bi(1)−S(1)	152.6(3)	N(3)−Bi(2)−O(41)	136.0(5)	O(11)−Bi(1)−O(13)	136.1(2)	O(23)−Bi(2)−N(3)	75.4(2)
N(2)−Bi(1)−S(1)	144.3(3)	O(31)−Bi(2)−N(4)	71.6(5)	N(1)−Bi(1)−O(13)	66.2(2)	O(31)−Bi(2)−N(3)	65.5(2)
O(44A)−Bi(1)−S(1)	109.2(3)	N(4)−Bi(2)−O(33)	139.6(5)	O(11)−Bi(1)−N(13)	76.2(2)	O(21)−Bi(2)−N(3)	134.2(2)
N(1)−Bi(1)−O(11)	65.5(4)	N(4)−Bi(2)−O(22)	140.8(4)	N(1)−Bi(1)−N(13)	133.2(2)	N(3)−Bi(2)−O(33)	63.0(2)
O(13)−Bi(1)−N(1)	68.0(5)	N(4)−Bi(2)−O(41)	63.2(4)	O(13)−Bi(1)−N(13)	137.2(2)	N(3)−Bi(2)−O(13B)	126.7(2)
N(1)−Bi(1)−O(21)	137.0(4)	O(43)−Bi(2)−N(4)	66.0(4)	O(11)−Bi(1)−O(22)	80.3(2)	N(3)−Bi(2)−O(1)	74.2(2)
N(1)−Bi(1)−O(23)	71.3(4)	O(31)−Bi(2)−O(33)	132.6(4)	N(1)−Bi(1)−O(22)	71.5(2)	O(23)−Bi(2)−O(31)	78.4(2)
N(1)−Bi(1)−O(44A)	131.0(4)	O(41)−Bi(2)−O(43)	128.8(5)	O(13)−Bi(1)−O(22)	86.3(2)	O(23)−Bi(2)−O(21)	133.6(2)
N(1)−Bi(1)−N(2)	120.0(5)	S(2)−Bi(3)−S(3)	84.0(2)	N(13)−Bi(1)−O(22)	133.2(2)	O(31)−Bi(2)−O(21)	84.5(2)
O(11)−Bi(1)−N(2)	125.5(4)	S(2)−Bi(3)−S(4)	169.3(2)	O(11)−Bi(1)−O(33A)	151.1(2)	O(23)−Bi(2)−O(13B)	73.9(2)
O(13)−Bi(1)−N(2)	83.0(5)	S(3)−Bi(3)−S(4)	86.5(2)	N(1)−Bi(1)−O(33A)	131.2(2)	O(31)−Bi(2)−O(13B)	144.0(2)
O(21)−Bi(1)−N(2)	62.9(4)	O(42)−Bi(3)−S(2)	100.3(3)	O(13)−Bi(1)−O(33A)	68.4(2)	O(21)−Bi(2)−O(13B)	98.2(2)
O(23)−Bi(1)−N(2)	62.8(4)	O(51)−Bi(3)−S(2)	94.0(4)	N(13)−Bi(1)−O(33A)	75.0(2)	O(23)−Bi(2)−O(33)	78.3(2)
O(44A)−Bi(1)−N(2)	68.0(4)	O(53)−Bi(3)−S(2)	87.3(4)	O(22)−Bi(1)−O(33A)	122.3(2)	O(31)−Bi(2)−O(33)	127.2(2)
O(13)−Bi(1)−O(11)	133.2(4)	N(5)−Bi(3)−S(2)	98.9(3)	O(11)−Bi(1)−O(21)	72.9(2)	O(21)−Bi(2)−O(33)	142.5(2)
O(11)−Bi(1)−O(21)	152.6(4)	O(42)−Bi(3)−S(3)	77.9(3)	N(1)−Bi(1)−O(21)	112.5(2)	O(13B)−Bi(2)−O(33)	68.8(2)
O(11)−Bi(1)−O(23)	71.1(4)	O(51)−Bi(3)−S(3)	148.9(4)	O(13)−Bi(1)−O(21)	125.1(2)	O(23)−Bi(2)−O(1)	146.7(2)
O(13)−Bi(1)−O(23)	99.2(5)	O(53)−Bi(3)−S(3)	80.8(4)	N(13)−Bi(1)−O(21)	86.2(2)	O(31)−Bi(2)−O(1)	77.0(2)
O(13)−Bi(1)−O(21)	70.2(4)	N(5)−Bi(3)−S(3)	145.9(4)	O(22)−Bi(1)−O(21)	48.1(2)	O(21)−Bi(2)−O(1)	65.5(2)
O(23)−Bi(1)−O(21)	125.5(4)	O(42)−Bi(3)−S(4)	72.8(3)	O(33A)−Bi(1)−O(21)	107.6(2)	O(33)−Bi(2)−O(1)	99.3(2)
O(11)−Bi(1)−O(44A)	72.1(4)	O(51)−Bi(3)−S(4)	91.7(4)	O(13B)−Bi(2)−O(1)	136.7(2)	O(2)−Bi(2)−O(31)	145.2(2)
O(13)−Bi(1)−O(44A)	150.6(4)	O(53)−Bi(3)−S(4)	96.0(4)	O(2)−Bi(2)−O(1)	70.9(2)	O(2)−Bi(2)−O(33)	72.2(2)
O(44A)−Bi(1)−O(21)	91.3(4)	N(5)−Bi(3)−S(4)	91.7(3)	O(2)−Bi(2)−O(21)	70.4(2)	O(2)−Bi(2)−N(2)	116.2(2)
O(44A)−Bi(1)−O(23)	72.7(4)	O(51)−Bi(3)−O(53)	130.2(4)	O(2)−Bi(2)−O(23)	136.3(2)	O(2)−Bi(2)−N(3)	118.2(2)

due to the OH vibration of water and NH vibrations of the sulfur-containing ligands. The carboxylate stretching vibrations are illustrated by the corresponding bands at 1580−1605 and 1370−1395 cm^{-1} and are partially overlapped by the NH_2 bending vibration and the CS stretching frequency. For **1** a shoulder around 1705 cm^{-1} is attributed to the protonated carboxylate group of the dipicolinate ligand. The metal−sulfur bond is assumed to be responsible for the shifting of the CS and CN vibrations at 1405−1430 cm^{-1} and 720−765 cm^{-1} to the lower wavelength region.

Compound **1** crystallizes in the triclinic space group $P\bar{1}$ as a centrosymmetric dimer with three Bi(III) atoms in the asymmetric unit (Figure 1). This compound is a discrete hexanuclear molecular complex in which the multinuclear framework is created by donation of a carboxylate oxygen atom of a $pydc^{2-}$ ligand chelating one bismuth atom to an adjacent bismuth atom. Examination of the charge balance required for complex **1** indicates that two of the dipicolinate ligands must be monoprotonated. Since all bismuth ions should be Bi^{3+}, a total of 18 negative charges would be required for formation of the neutral complex. This can only be achieved with a combination of eight $pydc^{2-}$ and two $Hpydc^{-}$ ligands giving $Bi_6(pydc)_8(Hpydc)_2(tu)_8$. The crystal structure suggests that a proton is attached to O(24) of the dipicolinate ligand coordinated to Bi(1) (Figure 1). Since the hydrogen atoms were not observed directly in the single crystal X-ray experiment, the assignment was based on the C−O bond distances and the short O(24)···O(54B) distance of 2.545(2) Å. The low solubility of the complex prevented collection of meaningful NMR data to address this issue.

In **1**, each $H_npydc^{(2-n)-}$ moiety acts as a conventional tridentate O,N,O ligand toward one of the three Bi(III) atoms. Two $H_npydc^{(2-n)-}$ ligands are bound to both Bi(1) and Bi(2) while only one such ligand is attached to Bi(3). The tu ligands are unevenly distributed. One tu ligand is attached to Bi(1), none to Bi(2), and three to Bi(3). The molecule can be considered to be composed of three types of fragments. Bi(1) forms a neutral [Bi(pydc)(Hpydc)(tu)] fragment (**I**), while the Bi(2) and its symmetry counterpart constitute the central core of the molecule forming a dianionic dimer $[Bi(pydc)_2]_2^{2-}$ (**II**). The third fragment centered on Bi(3) is a $[Bi(pydc)(tu)_3]^{+}$ cation (**III**). To assemble the molecules, two **I** fragments are attached to **II** such that one O atom of a $pydc^{2-}$ ligand that chelates to Bi(2) donates to Bi(1), while one O atom on a $pydc^{2-}$ ligand bound to Bi(1) donates to the symmetry related Bi(2). Two **III** units are attached to the central **II** via a single donor bond from another O atom on the a $pydc^{2-}$

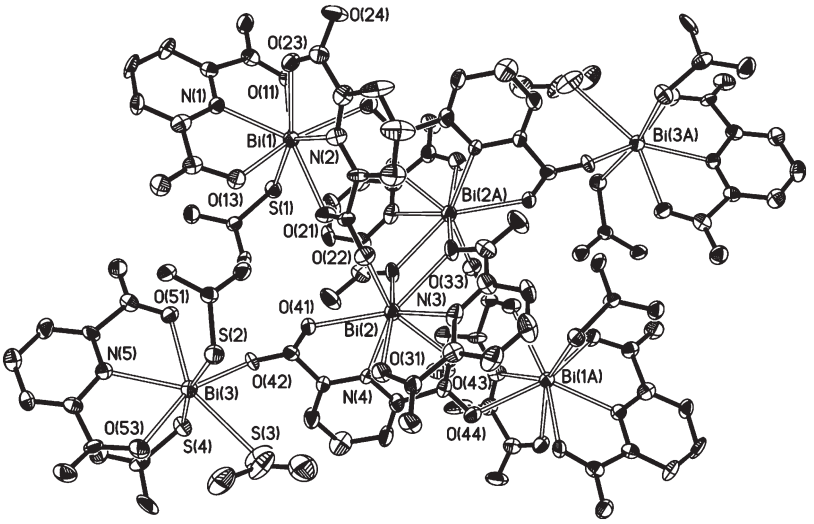

Figure 1. Coordination environment of Bi(III) in **1** with thermal ellipsoids at the 30% probability level. The hydrogen atoms were omitted for clarity.

ligand attached to Bi(2). There are no bridging ligands between Bi(1) and Bi(3). This arrangement gives coordination numbers (CNs) for Bi(1), Bi(2), and Bi(3) of 8, 8, and 7, respectively.

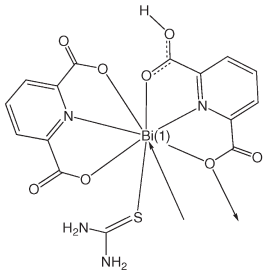

I

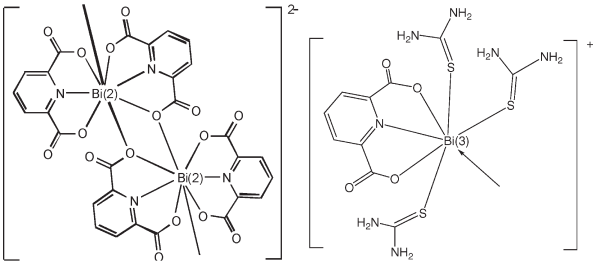

II **III**

The bismuth−sulfur bond in **I** of 2.743(5) Å is slightly shorter than the Bi−S distances found in fragment **III**, where the values range from 2.809(6) to 2.890(7) Å. These values are somewhat shorter than the usual range of Bi−S bonds in mixed-ligand tu-polyaminopolycarboxylate complexes (~3.0 Å and above).[29] The Bi−N and Bi−O distances associated with the chelating bonding mode of the $H_npydc^{(2-n)-}$ ($n = 0, 1$) ligands span a large range of values and probably reflect distortions caused by the involvement of the $H_npydc^{(2-n)-}$ ligands in bridging to other metal centers. In fragment **III**, where no additional bridging interactions are observed, the Bi−N distance is 2.51(1) Å and the Bi−$O_{carboxylate}$ values are 2.43(1) and 2.48(1) Å. The Bi−N distances in fragment **II** are statistically about the same as in fragment **III**, at 2.44(1) and 2.45(1) Å, but show asymmetric Bi−O distances: 2.29(1), 2.54(1) and 2.38(1), 2.52(1), indicating a skewing of the ligand toward one of the carboxylate groups. The average values of the Bi−O distances are very similar (for Bi(1) the value is 2.44 Å, as compared to 2.42 and 2.45 Å for Bi(2)) so that the shorter Bi−O distance on one side is compensated for by a longer Bi−O interaction to the remaining carboxylate. For Bi(1), the values are more irregular. For fragment **I**, one Bi−N distance is similar to those in fragment **III** (2.45(1) and 2.44(1) Å), but the other is very long (2.61(1) Å). For the latter $pydc^{2-}$ ligand, the Bi−O distances are also on the longest of these distances, being 2.58(1) and 2.57(1) Å, while those involved in the other $pydc^{2-}$ ligand show similar values and asymmetry as those seen in fragment **II** (2.34(1) and 2.49(1), average = 2.42 Å).

Compound **2** is a one-dimensional coordination polymer that shows similar bonding features to **1**. It consists of $[Bi_2(pydc)_3(tsc)(H_2O)_2]$ units assembled via bridging carboxylate groups into chains. The asymmetric unit of the crystal lattice is shown in Figure 2 with a fragment of the one-dimensional chain given in Figure 3. There is also a lattice water molecule that is involved in hydrogen bonding between the chains. The structure can be viewed as alternating $[Bi(pydc)(tsc)]^+$ (**IV**) and $[Bi(pydc)_2(H_2O)_2]^-$ (**V**) fragments.

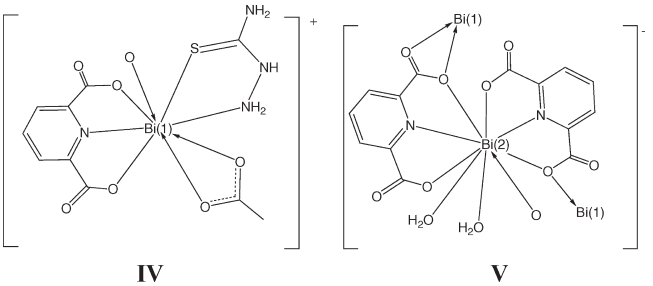

IV **V**

As with **1**, the $pydc^{2-}$ ligands adopt the usual O,N,O chelating mode with one attached to Bi(1) and two to Bi(2).

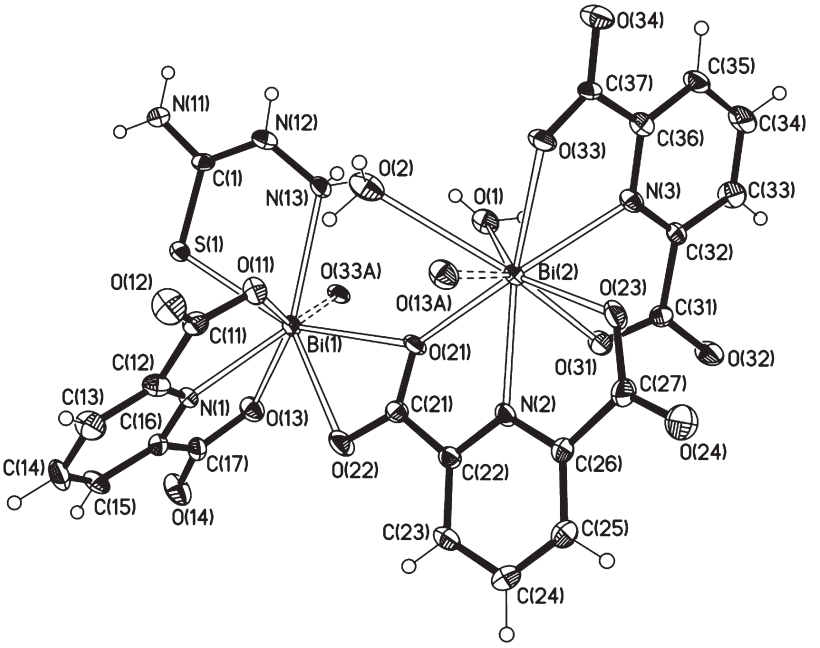

Figure 2. Coordination environment of Bi(III) in **2** with thermal ellipsoids at the 40% probability level.

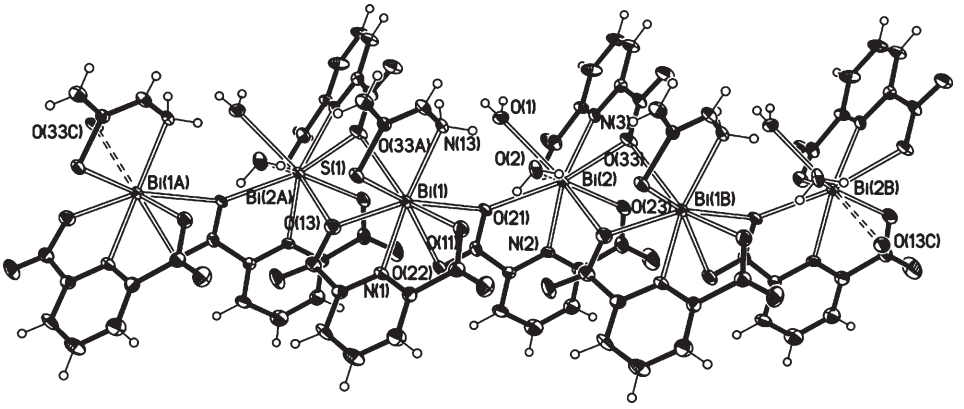

Figure 3. Fragment of the polymeric chain in **2**.

A bidentate, chelating tsc ligand is also attached to Bi(1), while two water molecules are attached to Bi(2). The polymeric nature of the molecule is created by two oxygen atoms of a single carboxylate on one $pydc^{2-}$ ligand attached to Bi(2) being donated to Bi(1) as seen in Figure 2. This gives CNs for the two independent Bi^{3+} ions of 8 and 9, respectively. The bismuth−nitrogen distances are similar to the shortest values found for compound **1**: Bi(1)−N(1) 2.378(7) Å, Bi(2)−N(2) 2.412(6) and 2.493(7) Å. The $Bi-O_{carboxylate}$ distances are asymmetric: Bi(1)−O(11) 2.278(7) Å, Bi(1)−O(13) 2.436(6) Å; Bi(2)−O(21) 2.488(5) Å; Bi(2)−O(23) 2.335(5) Å; Bi(2)−O(31) 2.399(6) Å; Bi(2)−O(33) 2.591(6) Å. The Bi−S distance (2.670(2) Å) in the bound tsc ligand is substantially shorter than those found for the tu ligands in compound **1**, which could be a reflection of the stronger chelating interaction. Similar results were reported for other bismuth(III)−tsc chelated complexes.[30] The nitrogen atom of the tsc ligand binds to Bi(1) at 2.620(7) Å, while Bi(2) is also coordinated by two water molecules at very different distances: 2.666(6) and 2.945(7) Å. The shorter distance is close to the average $Bi-O(H_2O)$ distance in bismuth(III) APC and PAPC complexes (2.71 Å). The polymeric nature of the structure is achieved by alternation of the **IV** and **V** fragments. In this arrangement, Bi(1) gains three additional O donor atoms, one from a neighboring fragment **V** and two from the other. In the latter case, the two O atoms chelate Bi(1) and are part of the same carboxylate group on a $pydc^{2-}$ ligand attached to Bi(2). The other O donor is also from a $pydc^{2-}$ ligand attached to Bi(2), but in this case that atom is also the atom of the carboxylate that is bound to Bi(2). The Bi(1)−O(33A) for this arrangement is 2.735(6) Å, and the $pydc^{2-}$ attached to Bi(1) donates in the reverse direction to the Bi(2) atom (Bi(2)−O 2.577(7) Å), giving a Bi_2O_2 ring structure. In complex **2** there are also weak slipping $\pi-\pi$ stacking interactions between the N1−C12−C13−C14−C15−C16 pyridine rings of the pydc ligand from two parallel polymeric chains. The projection of one ring into

(30) Battaglia, L. P.; Bonamartinicorradi, A.; Nardelli, M.; Vidonitani, M. E. *J. Chem. Soc., Dalton Trans.* **1978**, 583–587.

its parallel neighbor does not involve total eclipsing of all atoms; however, the corresponding C···C and C···N contacts are below 3.8 Å, the value suggested as the maximum limit for $\pi-\pi$ interactions.[31] The centroid-to-centroid distance between the aromatic rings is 3.672(7) Å, while the corresponding interatomic contacts are within 3.662(7)−3.689(7) Å.

In the crystal packing of both compounds the molecules are linked by hydrogen-bond interactions involving the carboxylate, tu or tsc donor atoms and, in the case of compound **2**, water molecules. The presence of a protonated carboxylate group in **1** results in a strong intermolecular hydrogen bond O(24)−H(24A)···O54(B) with relatively short H(24A)···O(54B) and O(24)···O(54B) distances (1.81(1) and 2.545(2) Å). The NH_2 groups of the thiourea molecules are involved in additional N−H···O intra- and intermolecular hydrogen bonds with the oxygen atoms of carboxylate groups to further stabilize the complex (Figure S1, Supporting Information). The presence of water molecules in compound **2** leads to important differences in the manner the molecules are linked together. There are 11 hydrogen bonds of different types (O−H···O, O−H···N, O−H···S, and N−H···O) involved in the stabilization of the polymeric complex (Figure S2, Supporting Information). The hydrogen atoms of the water molecules are involved in three intra- and three intermolecular hydrogen bonds with O, N, and S atoms. Additionally, each hydrogen atom of the tsc ligand is involved in one intra- and four intermolecular hydrogen bonds with water and carboxylate oxygen atoms. The crystal packing of **2** is further stabilized by the $\pi-\pi$ stacking interactions between the polymeric chains.

The Bi−O and Bi−N distances in **1** and **2** correlate well with published Bi(III)−aminopolycarboxylate structures. For instance, in the dimeric structure of $[Bi(Hpydc)(pydc)(dmso)]_2$ (dmso = dimethylsulfoxide), each bismuth center is surrounded by six donors atoms from the $H_npydc^{(2-n)-}$ ions, a bridging oxygen atom from the neighboring complex, and one oxygen atom of a dmso molecule with the following geometric parameters: Bi−O 2.209(8)−2.507(6) Å; Bi−N 2.418(9) and 2.481(9) Å; $Bi-O_{bridging}$ = 2.577(4) Å, $Bi-O_{dmso}$ 2.613(6) Å).[29] $[\{BiCl(H_2O)(pydc)\}_2]_n$ contains Bi(III) in a distorted pentagonal bipyramidal environment with the equatorial plane composed of three donor atoms of a $pydc^{2-}$ ligand, an oxygen donor atom of a water molecule, and the Bi_2O_2 ring, while the axial sites are occupied by an oxygen atom of the neighboring $pydc^{2-}$ ligand and by a chlorine atom (Bi−O 2.365(3)−2.633(3) Å; Bi−N 2.384(4) Å; Bi−Cl = 2.562(1) Å). In $[pydaH]_2[Bi_2(pydc)_4(H_2O)_2]\cdot 4H_2O$ (pyda = pyridine-2,6-diamine) each metal center is coordinated by two $pydc^{2-}$ ions, a bridging carboxylate oxygen atom, and a water molecule (Bi−O 2.327(3)−2.589(3) Å; Bi−N 2.435(3) and 2.555(3) Å).[29] Similar dimeric anionic units were found in $(phenH)_2[Bi_2(pydc)_4(H_2O)_2]\cdot 5H_2O$ (phen = 1,10-phenanthroline) (Bi−O 2.247(4)−2.691(4) Å; Bi−N 2.414(4) and 2.466(4) Å).[32] In most of the cases the bridging carboxylate groups of the dipicolinate ligands display a monatomic bidentate coordination. In contrast to this, two types of carboxylate bridges can be identified in **1**: a bidentate biatomic $\kappa^1:\kappa^1:\mu_2$ type for C(21)O(21)O(22), C(41)O(41)O(42), and C(47)O(43)O(44) and a bidentate monatomic $\kappa^0:\kappa^2:\mu_2$ type for C(37)O(33)O(34). The two types of carboxylate bridges found in **2** are $\kappa^0:\kappa^2:\mu_2$ for C(17)O(13)O(14) and C(37)O(33)O(34) and the tridentate bridging mode $\kappa^1:\kappa^2:\mu_2$ for C(21)O(21)O(22).

Conversion of the Precursors to Bismuth Sulfide. The initial decomposition reactions of **1** and **2** were performed in the presence of oleylamine (OA). It is well established that aliphatic amines can provide control over the morphology of the metal chalcogenide NPs. However, heating **1** and **2** at 175 °C in OA produced a mixture of Bi_2S_3 nanorods and metallic bismuth submicrometer particles (refer to Figure S3 in the Supporting Information). The products of decomposition were identified by XRD measurements with Cu Kα radiation (Figure S4, Supporting Information). The powders obtained from **1** and **2** are constituted of Bi_2S_3 nanorods and nanowires with a diameter 10−25 nm and up to several micrometers long, while the Bi particles are generally several hundreds of nanometers in size. When small quantities of DT or OT were added to the reaction mixture, the decomposition leads exclusively to Bi_2S_3 as established by TEM and powder XRD. TEM studies (Figure S5, Supporting Information) showed the formation of a mixture of nanorods of various aspect ratios.

The decomposition of **1** and **2** in anisole in the presence of DT or OT resulted in formation of uniform crystalline plate-like nanorods. All peaks in the XRD can be indexed to the orthorhombic phase of bismuth sulfide (JCPDS 00-017-0320, Figure 4). Reaction time plays an important role in the crystal growth and formation of the particles. Figure 5 shows the bright field (BF) TEM images of the NPs synthesized from **1** in the presence of DT and OA at different reaction times. When the reaction time is less than 4 min, the color of the solution does not change, and the decomposition reaction does not occur. After 4 min at 120 °C the color of the solution starts to change from yellow to brown. The color becomes darker as the reaction progresses, indicating the formation of Bi_2S_3. Figure 5A,B demonstrates that at the initial stage of the reaction small agglomerated NPs are formed in both DT and OT reactions. Selected area electron diffraction (SAED) patterns reveal that the particles are amorphous for short reaction times (see insets in Figure 5A1,B1). After 10 min the cores of the particles continue to grow, but the particles are still aggregated. There is a small difference between the DT and OT reactions under these conditions; agglomerated NPs in OT are still amorphous while some agglomerated NPs made in the presence of DT

(31) Janiak, C. *J. Chem. Soc., Dalton Trans.* **2000**, 3885–3896.

(32) Sheshmani, S.; Kheirollahi, P. D.; Aghabozorg, H.; Shokrollahi, A.; Kickelbick, G.; Shamsipur, M.; Ramezanipour, F.; Moghimi, A. *Z. Anorg. Allg. Chem.* **2005**, *631*, 3058–3065.

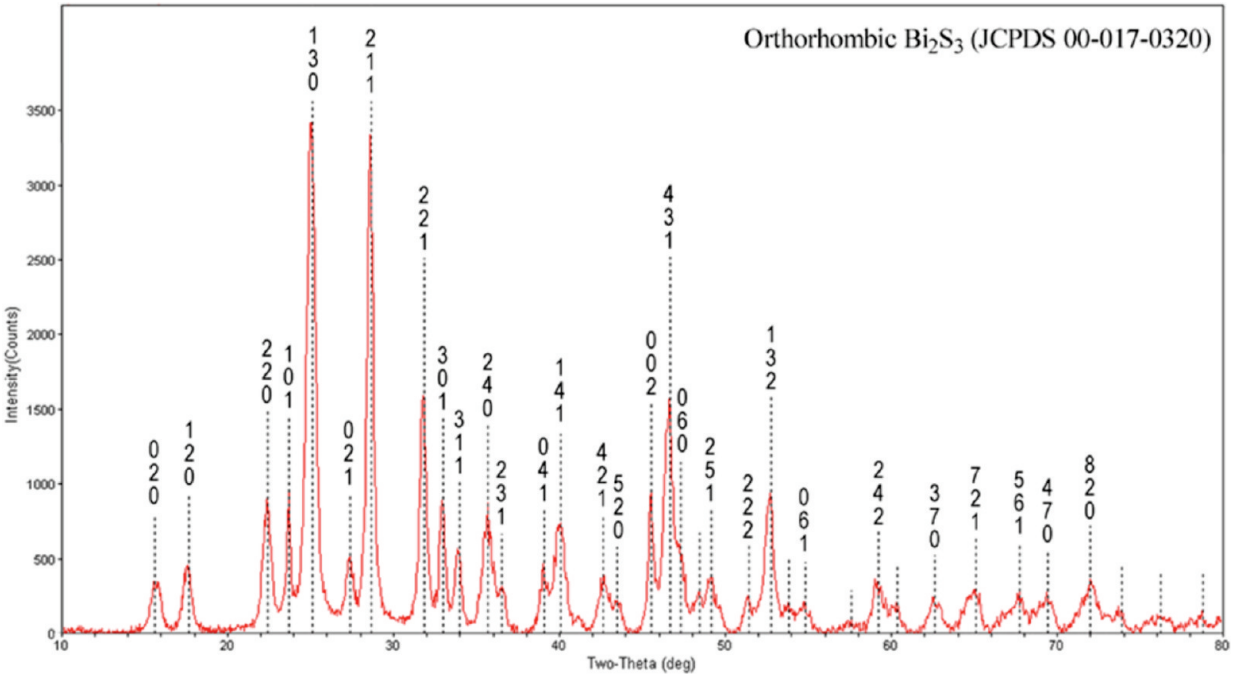

Figure 4. Representative powder XRD of the Bi_2S_3 nanorods prepared in the presence of thiols.

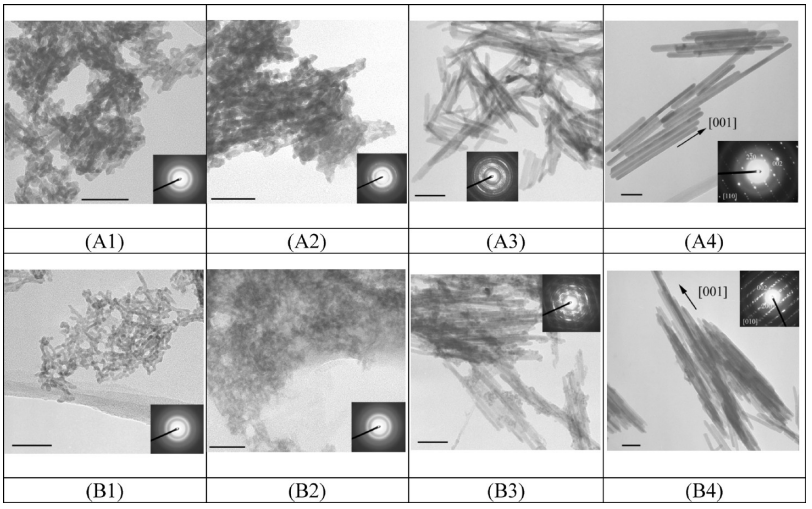

Figure 5. BF TEM images of the Bi_2S_3 particles obtained by decomposition of **1** in anisole in the presence of DT (A1−A4) and OA (B1−B4): after 4 min, 10 min, 1 h, and 16 h, respectively. The scale bar is 50 nm in all cases. The inset diffraction patterns are provided in larger size in the Supporting Information (Figure S7).

have become crystalline (see SAED patterns as insets in Figure 5A2,B2). After 1 h a large number of nanofibers with a diameter of 5−10 nm starts to appear. In addition to nanofibers, there are round nanoparticles less than 5 nm in diameter from the OT reaction. The SAED patterns (insets in Figure 5A3,B3) show that the nanofibers are crystalline for both OT and DT under these conditions. Nevertheless, polycrystalline SAED patterns from nanofibers in the DT reaction (Figure 5A3) look more clear than those prepared in OT (Figure 5B3), which may arise from the presence of the small amorphous, round nanoparticles in that sample. After 16 h at 120 °C nanorods of uniform diameter of 15−20 nm and sizes up to several hundreds of nanometers are formed in both DT and OT reactions. During the reaction process, the small amorphous nanoparticles may redissolve and contribute to the growth of crystalline well-defined nanorods through an Ostwald-type ripening process.[13] Simple crystal splitting of nanorods was observed in samples prepared in both DT and OT. In the case of the DT reactions the nanorods are more uniform in size and better shaped as compared to those prepared in the presence of OT. The diameters of the nanorods formed in the DT reaction (Figure 5A4) range from 10 to 20 nm, and lengths run from 250 to 400 nm. Multiple splitting of nanorods in the OT reaction caused azimuthal deviations of reflections in the SAED patterns (inset in Figure 5B4). The EDS data confirmed the presence of Bi and S in the particles (Figure S6, Supporting Information). The polycrystalline and single crystal SAED patterns showed that this is single

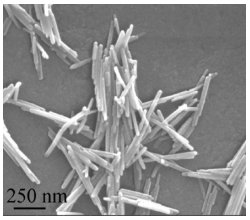

Figure 6. SEM image of the Bi_2S_3 particles obtained by decomposition of **2** in anisole in the presence of DT after 48 h at 120 °C.

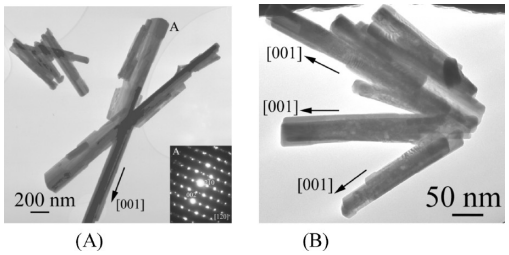

Figure 7. BF TEM images of the Bi_2S_3 particles obtained by hydrothermal decomposition of **1**. (A) Image showing the single crystal nature of the particle but with widely varying sizes. (B) Particles growing from the same core but all showing growth in the same crystallographic direction, [001]. The inset in Figure 7A is provided in larger scale in the Supporting Information (Figure S9).

phase Bi_2S_3 (orthorhombic, *Pbnm*, $a = 11.15$ Å, $b = 11.30$ Å, $c = 3.98$ Å; Figures S7 and S8, Supporting Information). It has been established that longer reaction times result in only a slight increase in the aspect ratio of the nanorods (Figure 6).

The decomposition reactions of **1** and **2** under hydrothermal conditions in the presence of CTAB produced nanorod-like Bi_2S_3 particles from ~50 nm to several hundreds of nanometers in diameter and to several micrometers in length (Figure 7A). The BF TEM micrograph in Figure 7B shows growth of nanorods from the same core. The generation of intergrown nanorods may involve the formation of amorphous "growing seeds" during the decomposition of the precursors, followed by the production of crystalline nanonuclei and preferential growth of [001]-oriented Bi_2S_3 nanorods, controlled by the surfactant.[17] There is no significant difference in the behavior of the two complexes, which suggests similar rates of crystallization for Bi_2S_3 under hydrothermal conditions at 175 °C. Whereas there are no significant differences in the morphology of the resulting particles obtained from the two complexes, the yield of the particles obtained from **2** is significantly lower, which is probably due to its lower S:Bi ratio. The significant variation in particle sizes may be explained by uneven deposition rates during the hydrothermal process. Similar results were reported by Chen et al.[33]

Solvothermal decomposition of **1** and **2** with an OA−oleic acid mixture in the presence of small amounts of DT resulted in bundles of Bi_2S_3 nanorods. Figure 8 shows representative (BF TEM) images of such Bi_2S_3 nanostructures. The individual nanocrystals have diameters

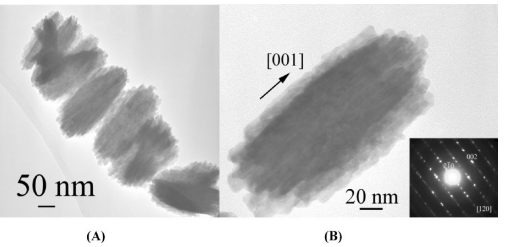

Figure 8. BF TEM images of the Bi_2S_3 nanorods bundles.

between 85 and 120 nm and are up to ~300 nm in length. The XRD pattern of the prepared nanocrystals shows sharp peaks corresponding to orthorhombic bismuthinite phase (Figure 4). The individual nanorods inside bundles have diameters of ~10 nm, while the diameters of the bundles range from 90 to 120 nm with lengths up to ~300 nm. The SAED patterns recorded from individual nanorods (insets in Figures 5G,H and 7A) and bundles (inset in Figure 8B) reveal that the direction of growth is always the same [001]. Several research groups recently reported similar observations.[12,13,15,16,20,34−36] Sigman and Korgel synthesized orthorhombic Bi_2S_3 nanorods and nanowires by the solventless thermolysis of bismuth alkylthiolate precursors.[36]

Tang and Alivisatos have recently reported the crystal splitting of Bi_2S_3 NPs obtained by reacting a bismuth−oleic acid complex with elemental sulfur in 1-octadecene.[28] It was suggested that the bismuthinite nanocrystals may form by a similar splitting crystal growth mechanism as in the case of minerals in nature.[28] The authors proposed a growth mechanism for the split Bi_2S_3 nanofibers or nanorods with a preferential growth direction along the *c*-axis associated with its lamellar structure.[28] Along the lamellar lines in [001] direction, we always observed long-range strain diffraction contrast inside the individual nanorods, which is better identified at higher resolution (Figure 9A, lines A−C). HRTEM images (Figure 9B,C) show that this long-range strain diffraction contrast is caused by a variety of crystal defects: linear defects (dislocations), planar defects (stacking faults), and atomic distortions (displacements of atoms from their regular positions). This means that the crystal lattice in these areas is under strong stress. On the basis of these observations we suggest that (1) these defects are formed during nanocrystal growth similar to that of crystal growth in nature and (2) the strain field caused by presence of these defects is the origin of the nanocrystal splitting.

The density of such defects may have a correlation with the speed of growth—faster growth is expected to cause a higher density of defects in the structures. It is well-known that crystal splitting is more pronounced in systems with rapid crystal growth, which tends to occur in supersaturated solutions. One can argue that similar processes might occur under solvothermal conditions during the

(33) Chen, R.; So, M. H.; Che, C. M.; Sun, H. Z. *J. Mater. Chem.* **2005**, *15*, 4540–4545.
(34) Zhu, G.; Liu, P.; Zhou, J.; Bian, X.; Wang, X.; Li, J.; Chen, B. *Mater. Lett.* **2008**, *62*, 2335–2338.
(35) Zhang, H.; Wang, L. *Mater. Lett.* **2007**, *61*, 1667–1670.
(36) Sigman, M. B.Jr.; Korgel, B .A. *Chem. Mater.* **2005**, *17*, 1655–1660.

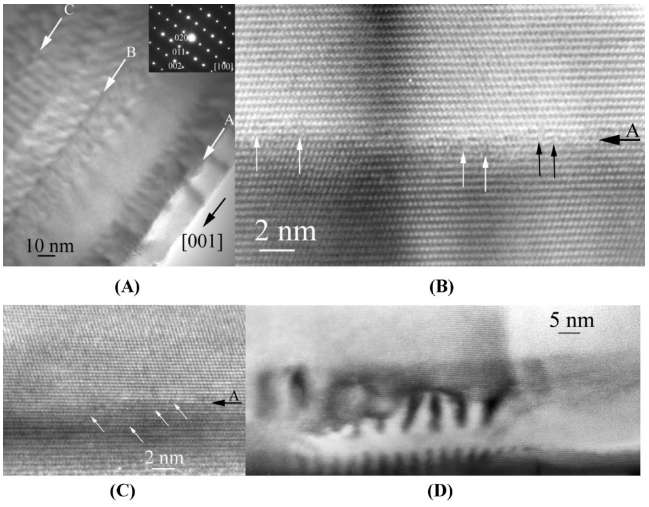

Figure 9. HRTEM images of a Bi_2S_3 nanoparticle showing a variety of structural defects. (A) Image showing long-range deformation contrast caused by the presence of defects along the [001] direction (arrows A−C). (B) Black arrows point out dislocations and white arrows atomic distortions. (C) The white arrows indicate planar defects (stacking faults). (D) Image showing the origin of split rods along one of the lines where the defects have collected.

synthesis of the particles depicted in Figure 8. The combination of weakly and strongly binding surfactants present in the reaction mixture could affect the growth process and favor crystal splitting. It has been widely accepted that the tendency of bismuthinite to form rod-like morphologies is due to its inherent Bi−S chain structure. Our group has recently reported crystal splitting in Fe_2P NPs[37] having rod-like, haystack, dumbbell, and spherulitic morphologies. A common feature for the both the Bi_2S_3 and Fe_2P systems is the presence of oleic acid, which is believed to facilitate crystal splitting.[28]

The morphology of the particles obtained form compounds **1** and **2** may be explained by a combination of extrinsic and intrinsic factors. The intrinsic reason results from the chain-type crystal structure of bismuthinite with strong covalent bonds along the *c* crystallographic axis and much weaker van der Waals bonding between the chains of the layered structure.[1] This will favor a higher growth rate along one direction and facilitate a one-dimensional nanostructure formation by an anisotropic growth habit along the *c* axis.[12,13,15,16,20,34,35] The dipicolinate ligand is attached strongly to Bi(III) and thus stabilizes the complex, that is, no decomposition reactions with tu or tsc occur in hot aqueous media. At higher temperatures in the presence of various surfactants the thio-containing ligands react with the Bi(III) ions to form the initial Bi_2S_3 crystalline seeds. The surfactants can act as capping agents for the initial NPs and thus prevent their agglomeration. We believe that DT and OT play a major role in the one-dimensional NP formation due to the strong capping ability of the thiol groups associated with Bi(III). The differences in morphology of the NPs obtained by various synthetic routes are likely associated with the different affinity of the surfactants to the growing Bi_2S_3 NPs.

(37) Kelly, A. T.; Rusakova, I.; Ould-Ely, T.; Hofmann, C.; Lüttge, A.; Whitmire, K. H. *Nano Lett.* **2007**, *7*, 2920–2925.

Conclusions

Two new bismuth(III) mixed ligand carboxylate−thiourea or thiosemicarbazide complexes have been prepared and their decompositions investigated by wet-chemical procedures. The air-stable precursors $[Bi_6(pydc)_8(Hpydc)_2(tu)_8]$ (**1**) and $\{[Bi_2(pydc)_3(tsc)(H_2O)_2]\cdot H_2O\}_\infty$ (**2**) are conveniently prepared from readily available starting materials. Both of these compounds produce Bi_2S_3 NPs under both aqueous and nonaqueous conditions. Several critical factors, including temperature, solvent, and capping molecules were identified as affecting the morphology of the resulting 1D nanostructures. It is indicated that at relatively low temperature (e.g., 120 °C) thiols as the capping molecules are beneficial for the formation of uniform Bi_2S_3 nanorods. The formation of rod-like Bi_2S_3 nanostructures is believed to occur through decomposition of the precursors and formation of initial Bi_2S_3 nuclei, which subsequently grow into nanorods of various morphology owing to Ostwald-type ripening and crystal splitting processes. The hydrothermal decomposition with CTAB resulted in intergrown nanorods, while the solvothermal reaction in OA and DT in the presence of oleic acid produced bundles of nanorods that are generated by crystal splitting, which is caused by the presence of linear and planar defects as well as atomic distortions created during growth of the nanocrystals. While both nanorods and bundles of nanorods have been observed previously for the bismuth sulfide system, this is the first report of detailed HRTEM images documenting the variety of crystal defects that lead to the observed splitting.

Acknowledgment. V.S. is thankful to Dr. Teyeb Ould-Ely and Dr. Cristina Hofmann for useful discussions and their help with some experiments. We gratefully acknowledge financial support from Welch Foundation (C-0976) and the National Science Foundation (DGE-0411679). The CRDF and MRDA also provided partial support of this project (Award MTFP-1015).

Supporting Information Available: CIF files giving crystallographic data for **1** and **2** as well as some additional characterization of the bismuth sulfide nanostructures (PDF). This material is available free of charge via the Internet at http://pubs.acs.org.